THE ASTROPHYSICAL JOURNAL, 340:1011–1023, 1989 May 15

THE RELATION BETWEEN X-RAY EMISSION AND ROTATION IN LATE-TYPE STARS FROM THE PERSPECTIVE OF X-RAY SELECTION[1]

THOMAS A. FLEMING[2]
Steward Observatory, University of Arizona
AND
ISABELLA M. GIOIA[3] AND TOMMASO MACCACARO[3]
Harvard-Smithsonian Center for Astrophysics
Received 1988 June 28; accepted 1988 October 24

ABSTRACT

We analyze an X-ray–selected sample of 128 late-type (F–M) stars. These stars were identified as optical counterparts to serendipitous X-ray detections made by the *Einstein Observatory* Extended Medium Sensitivity Survey. Once identified as X-ray sources, the sample was followed up by an extensive program of optical observations, including high-resolution and low-resolution spectroscopy and photometry. Spectral types, luminosity classes, distances, X-ray luminosities, projected rotation rates ($v \sin i$), radial velocities, and binary status have been determined for the sample.

We find that L_x is correlated with $v \sin i$ for single stars. The best fit yields $L_x \propto (v \sin i)^{1.05 \pm 0.08}$ for F7–M5 stars. A segregation between dwarfs and giants is not seen. However, L_x does not correlate with $\Omega \sin i$, which leads us to believe that the correlation seen with $v \sin i$ is actually a correlation with radius. Indeed, L_x correlates strongly with radius (color, mass) for main-sequence stars.

These results, which appear to be at odds with previous work, provide plausible evidence for saturated levels of stellar coronal activity. There exists an upper limit to the coronal activity exhibited by any late-type star which is determined by the star's radius and, hence, convection zone depth. An X-ray–selected sample of late-type stars will preferentially contain stars at this limit.

Subject headings: stars: late-type — stars: rotation — stars: X-rays

I. INTRODUCTION

Coronal X-ray emission from late-type stars (i.e., those with outer convective envelopes) is caused by nonradiative heating of the upper layers of a stellar atmosphere. The current view is that this process functions due to the presence of magnetic fields which are generated by a magnetic dynamo. The catalyst for such a dynamo is differential rotation and convective motions. Therefore, the obvious parameter to compare with stellar X-ray luminosity is stellar rotation.

The seminal paper on this topic was written by Pallavicini *et al.* in 1981. In it, the authors considered the correlation between soft X-ray luminosity (L_x) and projected rotational velocity ($v \sin i$) for a sample of 34 late-type (F–M), single stars. The sample was chosen from the Center for Astrophysics stellar survey program and other pointed-observation programs of various guest investigators to the *Einstein Observatory*. Rotational velocities were obtained from the literature. Consequently, this sample was optically selected and biased toward the selection criteria of the various *Einstein* observers and optical spectroscopists whose data were used.

Pallavicini *et al.* (1981, 1982) came to the following conclusions: (1) L_x did correlate with $v \sin i$ in stars of spectral type later than F7. The best fit to the data was $L_x = 10^{27}(v \sin i)^2$ ergs s^{-1}. (2) L_x did not correlate with L_{bol} for these same stars. This result was in contrast to their discovery that $L_x = 10^{-7} L_{bol}$ for a sample of O and B stars which they also analyzed. (3) They found no difference in X-ray behavior between luminosity classes III, IV, and V among the late-type stars. (4) The early F stars fitted neither correlation. They were overluminous in X-rays when placed on the early-type, L_{bol} relation and underluminous in X-rays when placed on the late-type, $v \sin i$ relation.

Other studies of optically selected samples have shown a relation between L_x and rotation in late-type stars, although of somewhat different form. Mangenay and Praderie (1984) found that a power-law relation between L_x and an effective Rossby number (i.e., a parameter which combines rotation rate with a parameter which characterizes the convection zone) fitted the data well for all spectral types. Marilli and Catalano (1984) claimed that the proper correlation was that L_x was an exponential function of rotation period. Other investigators have discovered departures from the Palavicini relation at rapid rotation rates for the F dwarfs (Walter 1983), the G dwarfs (Walter 1982), and late-type dwarfs in the Pleiades (Caillault and Helfand 1985; Micela *et al.* 1985). These authors suggest that the L_x versus $v \sin i$ relation flattens out at high rotational velocities.

We have decided to explore the relationship between L_x and rotation in late-type stars from a different perspective by using our X-ray–selected sample. In this way, we avoid the biases associated with the optically selected samples which were mentioned above. Instead, our sample is biased toward strong coronal activity (i.e., X-ray emission). This approach has not been tried before due to the lack of large, X-ray–selected, stellar samples and the enormous amount of ground-based observing time required to properly identify and follow up serendipitous X-ray detections. Indeed, other studies involving X-ray–

[1] Research done in part at the Multiple Mirror Telescope, operated jointly by the Smithsonian Astrophysical Observatory and the University of Arizona.
[2] Visiting Astronomer, Kitt Peak National Observatory, operated by Associated Universities for Research in Astronomy, Inc., under contract with the National Science Foundation.
[3] Also Istituto di Radioastronomia del CNR, Bologna, Italy.

selected samples of stars have suffered from small-number statistics (cf. Favata *et al.* 1988; Caillault *et al.* 1986). In the present study, this difficulty is overcome by using what we believe to be the largest and best optically observed, X-ray–selected sample of stars to date.

A description of the sample and the optical observations is given in § II. In § III, we attempt to correlate L_x with rotation and other optically derived parameters. The implications which our results have for theories of stellar coronal emission are discussed in § IV. Section V contains a summary.

II. OBSERVATIONS

The data base from which this sample of stars was defined was the *Einstein Observatory* Extended Medium Sensitivity Survey (EMSS; Gioia, Maccacaro, and Wolter 1987). This contains an unbiased sample of 835 X-ray sources which were detected serendipitously by the *Einstein Observatory* Imaging Proportional Counter (IPC; Gorenstein, Harnden, and Fabricant 1981). The central region of each IPC frame (circle having a 5′ radius around the target object) associated with a pointed observation was excluded from the sample in order to avoid selection biases. The size of the sample has greatly increased over the previously published MSS (Gioia *et al.* 1984; Maccacaro *et al.* 1982) due to the inclusion of more IPC fields and the reprocessing of detected sources down to the 4 σ level. Optical identification of the MSS sources showed that about 25% of them were associated with stellar objects in our Galaxy (Gioia *et al.* 1984; Stocke *et al.* 1983).

For convenience of observation, we have defined a subsample of the EMSS above $\delta = -20°$ for which the IPC data were reprocessed before 1985 August 15. This will not bias the sample, since the order in which the IPC frames were reprocessed was random with respect to stars. This subset includes 809 IPC fields covering 441 deg^2 of the sky (56% of the total EMSS) and yielding 471 serendipitous detections. The Palomar Observatory Sky Survey (POSS) was used to locate candidate optical counterparts within the X-ray position error circle. Error circle diameters typically ranged from 30″–60″ for most sources. Then, low-dispersion spectroscopy was obtained for as many of these objects as possible in order to identify the most likely X-ray source. A few sources were also observed with either the *Einstein Observatory* High Resolution Imager (HRI) or the *EXOSAT*. These sources have a positional accuracy of a few arcsec.

The primary criterion for identification was observation of a well-known class of X-ray emitting object (e.g., QSO, BL Lac, AGN, cluster of galaxies, dMe or dKe flare star, RS CVn binary, cataclysmic variable). When more than one star was located within an X-ray position error circle, stars which showed evidence of chromospheric activity (i.e., optical emission lines) or rapid rotation were identified with the X-ray source. Identifications based on these criteria were made irregardless of apparent magnitude or f_x/f_v ratio. When choosing among more than one "normal" star or "normal" stars and "normal" galaxies, the identification was made on the basis of the f_x/f_v ratio. Previous work on the MSS, for which reasonable identifications were found for 100% of the sources, has shown a dichotomy in apparent magnitude between Galactic and extragalactic identifications at $m_v \sim 16$ (Stocke *et al.* 1983; Maccacaro *et al.* 1988). This arises from the fact that f_x/f_v is small ($< 10^{-1}$) for most stellar objects. Therefore, stars dimmer than 16th mag generally have X-ray fluxes too faint to have been detected in the MSS.

This criterion can be used with great confidence for two reasons. First, the MSS was small enough that all possible counterparts on the POSS were observed spectroscopically. Second, many of the MSS source identifications were confirmed by reobservation with either the HRI or, at radio wavelengths, the Very Large Array (VLA).

To date, 74% of the sources in this EMSS subsample have been positively identified with either Galactic or extragalactic objects. Over a 2 yr period, we obtained extensive optical spectroscopy and photometry of the 137 stars identified with X-ray sources in this subsample, 128 of which are of spectral type F through M. Of the 124 sources not yet identified, only six have objects in the error box at or brighter than 16th mag. The rest have only objects fainter than 16th mag. We assume from the previous MSS work that they are probably extragalactic sources. The six unidentified sources associated with brighter objects are not positive identifications because f_x/f_v is too high for their spectral type. Thus, these could also prove to have extragalactic optical counterparts. On the other hand, these stars could have unseen M dwarf companions which are the true source of the X-rays, or the stars themselves could have unusually high X-ray luminosities or have been detected while flaring.

The last two paragraphs illustrate an important caveat in using this serendipity survey. Unless one has an accurate X-ray position, one is never quite sure if one has made the proper identification. Identifications can be made with various degrees of confidence, but the true X-ray detection could still be of an object below the POSS magnitude limit, or an unseen companion, or a combination of flux from more than one source. By using the f_x/f_v criterion, one eliminates the possibility of making an unusual discovery (e.g., an extremely X-ray–luminous, yet otherwise normal-looking star). Consequently, one cannot make grand statements and hypotheses based on individual objects from this sample. Only when analyzed statistically, based on trends seen in a large number of objects, can this sample be used to draw astrophysical conclusions.

The observational data for this EMSS subsample of stars consist of one soft X-ray (0.3–3.5 keV) flux, f_x, at the time of IPC detection and the following optical data for all members of the sample (except a few of the faintest of dwarfs): (1) 5 Å resolution spectroscopy covering $\lambda\lambda$3600–7600 for the red (K–M) stars only; (2) 2 Å resolution spectroscopy covering $\lambda\lambda$3600–6000; (3) 0.1 Å resolution echelle spectroscopy of the region around the Mg I *b* lines (5187 Å); (4) *UBVRI* photometry.

The low-resolution spectroscopy was obtained with spectrographs at the Multiple Mirror Telescope (MMT) on Mount Hopkins, AZ, the Steward Observatory 2.3 m telescope, and the No. 2 0.9 m telescope, both on Kitt Peak, AZ. The high-resolution spectroscopy was obtained with the echelle spectrographs at the MMT and 1.5 m Tillinghast reflector on Mount Hopkins, and the stellar spectrograph at the McMath Solar Telescope on Kitt Peak.

The photometry was obtained either with the Catalina Photometer at the Steward Observatory 1.5 m telescope on Mount Lemmon, AZ or with the Automated Filter Photometer (AFP2) at the No. 2 0.9 m telescope on Kitt Peak. Both filter sets were prescribed by Bessel (1976) with *UBV* on the Johnson system and *RI* on the Kron-Cousins system.

The low-resolution spectra were used to assign spectral types to each member of the sample, including stars already cataloged in the SAO and other bright star catalogs. This was

important, since the spectral types given in the SAO catalog were often inaccurate. All spectral types given in this paper were assigned by us. The MK classification system was used for all stars. The stars were classified by comparison to standards and calculation of feature ratios found in the catalogs of digital spectra of Turnshek *et al.* (1985), Jacoby, Hunter, and Christian (1984), and Turnshek (1981).

Distances to each star were calculated using trigonometric parallaxes when available. If not, photometric parallaxes were calculated using the M_V versus $(V-I)_{KC}$ relation of Reid and Gilmore (1982) for the K and M stars, and the M_V versus $(B-V)$ relation of Gliese (1982) for the F and G stars. The photometry was also used to verify the spectral type, to distinguish between luminosity classes, and to check for interstellar reddening. For a few stars, values of E_{B-V} and A_V were calculated. Those stars for which we were unable to obtain photometry, or which had photometry contaminated by another star, were assigned an M_V from the spectral type using the values given for standards in Boeshaar (1976) for the M stars and Mikami (1978) for earlier types.

After examining the spread in the M_V versus spectral type and color relations, we estimate the errors in M_V to be 1.0 mag for spectroscopic parallaxes and 0.4–0.6 mag for photometric parallaxes. Given the errors in our measurement of V (typically 0.1–0.2 mag), this translates into a typical error of 46% and 18%–28% in distance, respectively. The error in these relations is much larger than the error in M_V introduced by the error in measuring colors or by misclassifying a star by one subtype. Errors in M_V for trigonometric parallaxes are usually on the order of 0.1 mag (10% in distance).

The soft X-ray flux, f_x, was derived from corrected IPC counts s^{-1} by assuming a thermal spectral distribution with metallic emission lines (Raymond and Smith 1977). The conversion factor adopted here is 2×10^{-11} ergs cm^{-2} $count^{-1}$. The f_x was also corrected for any interstellar absorption that was evident from the optical photometry. Errors in f_x were computed using Poisson statistics on the number of IPC counts and were typically on the order of 20%. The soft X-ray luminosity, L_x, was computed for each star assuming isotropic emission. The 1 σ errors which are quoted for L_x in Tables 1 and 2 were computed by propagating the errors in both f_x and the distance for each star.

Furthermore, there were five EMSS sources which had two Me dwarfs (not always associated) in the IPC error circle. If both stars were at the same distance and had the same rotation rate, then the X-ray flux was divided between them in proportion to L_{bol} since L_x/L_{bol} is essentially constant for M dwarfs (Ruciński 1984; Fleming *et al.* 1988). If not, the total X-ray flux was assigned to each star, and they are marked as upper limits in all tables and figures.

The 0.1 Å resolution echelle spectroscopy centered at 5187 Å was used to measure rotation rates ($v \sin i$) and radial velocities for each star. Both quantities were measured using the cross-correlation technique of Tonry and Davis (1979) with the templates described by Latham (1985). The manner in which we measure rotation rates and estimate errors is identical to that described by Hartmann *et al.* (1986). The echelle resolution limits the ability to measure rotation below 10 km s^{-1}. Zero-point corrections to the radial velocities were determined by observing IAU standards (Bouigue 1973) as well as the dawn and dusk skies.

This last measurement was made at several epochs for each star in order to look for variations in radial velocity which are characteristic of short-period, "astrophysical" binaries. In this study, we wish to keep such binaries separate from the single stars.

The stellar parameters which are directly used in this paper are listed in Tables 1 and 2. Data for the apparently single stars are tabulated in Table 1, while Table 2 contains the binary star data. The first column contains the EMSS source name, while other catalog designations are given in the next column. Spectral type is listed in the third column. The adopted values for stellar radius (as described in § III*a*) are listed in the fourth column, and the measured values of L_x and $v \sin i$ are in the fifth and sixth columns.

A complete compilation of all the observational data on the EMSS stellar sample can be found in Fleming (1988). A larger listing of data on the M dwarfs, as well as a more extensive treatment, has already been published (Fleming *et al.* 1988).

III. ANALYSIS

The four pre–main-sequence (PMS) stars listed in Tables 1 and 2 are excluded from the following analysis since there are so few of them and PMS stars may have a radically different mechanism for emitting X-rays compared to dwarfs and giants (see the review by Rosner, Golub, and Vaiana 1985).

a) Single Stars

We begin the rotation/X-ray analysis with the apparently single stars. This refers to those members of the sample which showed no evidence for radial velocity variation. In Figure 1, L_x is plotted against $v \sin i$ for these stars. As was mentioned in the previous section, the resolution of the echelle spectra prevent us from measuring $v \sin i$ accurately below 10 km s^{-1}. Consequently, those stars in our EMSS subsample for which $v \sin i < 10$ km s^{-1} will be of little use in determining the relation between $v \sin i$ and L_x. However, we plot them in Figure 1 in one bin at $v \sin i = 5$ km s^{-1} to see if they generally have values of L_x less than those stars for which $v \sin i > 10$ km s^{-1}.

After eliminating the stars which are dubious X-ray sources (i.e., those stars whose positional error circles contain other possible stellar or extragalactic contributors to the X-ray detection), there are 16 stars in the low-rotation bin which have $L_x > 10^{29}$ ergs s^{-1}. This is the X-ray luminosity one would expect a star rotating at $v \sin i = 10$ km s^{-1} to have from the Pallavicini *et al.* relation. Half of these stars fit well within the scatter about the Pallavicini *et al.* relation. Of greatest concern are the stars which have $v \sin i < 10$ km s^{-1} and $\log L_x > 30.5$ ergs s^{-1}. There are no single stars in the sample of comparable X-ray luminosity which have $v \sin i > 10$ km s^{-1}. However, one must remember that we have identified the binaries in our sample from radial velocity variations. Any binary systems whose orbital axes are inclined towards the line of sight would be included in the low-rotation bin in Figure 1. Since there are identified binaries in our sample which do have such high X-ray luminosities, it is reasonable to assume that the X-ray "bright" stars in the low-rotation bin of Figure 1 are binaries.

In order to retain a proper sense of scale, we have added the data for the late-type stars which were used by Pallavicini *et al.* to Figure 1. We plot the data for all single stars of spectral types F0–M5 (excluding PMS stars) in Figure 1*a*, while we exclude the points which represent the early F stars (F0–F6) from Figure 1*b*. These figures show that, while some of the EMSS stars fall along the $L_x \propto (v \sin i)^2$ relation, others fall well below it. In addition, the early F stars from the EMSS

TABLE 1

APPARENTLY SINGLE STARS

EMSS	Other (HD)	Sp. Type	R (10^5 km)	L_x (10^{29} ergs s^{-1})	v sin i (km s^{-1})
1E0215.0+1813	14147	F0 V	13.42	2.15 ± 2.02	24 ± 5.9
1E1254.9+0142	112542	F4 V	12.58	1.42 ± 1.33	22 ± 0.9
1E0031.9−0646	3126	F4 V	12.58	4.91 ± 1.88	26 ± 2.0
1E2335.3+0305	222111	F5 V	10.46	3.79 ± 3.52	< 10
1E1634.8+2638	149931	F5 V	9.99	9.03 ± 3.35	< 10
1E0356.9+1011	25102	F5 V	9.54	1.05 ± 0.40	49 ± 3.8
1E1704.3+5432	154905	F6 V	7.11	1.31 ± 0.31	20 ± 1.0
1E1635.0+2651	149973	F6 V	9.15	3.42 ± 1.28	34 ± 1.2
1E0758.8+1411	65916	F6 IV	9.11	10.54 ± 9.90	13 ± 1.6
1E0333.1+0607	...	F6 V	10.46	9.82 ± 9.22	24 ± 1.5
1E0103.6+3206	...	F6 V	10.46	10.16 ± 4.36	39 ± 4.7
1E0851.2+2025	SAO80493	F7 V	10.46	2.89 ± 2.67	26 ± 1.7
1E1521.2+3027	137107	F8 V	6.91	0.08 ± 0.02	3
1E2034.9+7532	...	F8 V	8.12	10.97 ± 4.37	29 ± 2.2
1E2045.4+7523	198547	F8 V	9.54	4.01 ± 1.54	60 ± 6.0
1E0538.6−0949	37827	F8 V	9.54	2.04 ± 1.95	65 ± 5.6
1E1457.0+2108	...	F8 V	7.58	13.34 ± 5.89	< 10
1E0448.4+1058	30810	F8 V	7.41	0.97 ± 0.33	< 10
1E0308.4+1413	...	F8 V	9.54	41.14 ± 38.09	< 10
1E0132.5+2101	...	F9 V	7.76	5.70 ± 2.39	28 ± 1.4
1E1621.5+2640	...	G0 V	4.22	101.04 ± 94.94	< 10
1E1330.6−0811	117860	G0 V	8.50	1.64 ± 1.52	< 10
1E0830.3+1126	72429	G0 III	51.71	70.80 ± 65.94	14 ± 0.7
1E0235.6+1631	...	G1 V	7.47	85.99 ± 80.60	< 10
1E2136.1−1509	...	G1 V	7.51	88.96 ± 83.55	< 10
1E0036.1+3309	...	G2 V	6.98	11.42 ± 5.03	26 ± 1.5
1E1153.0+2344	...	G2 V	6.66	94.64 ± 38.53	< 10
1E0830.7+2828	...	G4 V	3.00	5.40 ± 2.36	< 10
1E0411.5+2327	26736	G5 V	6.13	0.78 ± 0.35	< 10
1E0402.4+2152	25680	G5 V	6.02	0.37 ± 0.06	3
1E0820.2+0201	70573	G6 V	6.88	1.35 ± 0.55	14 ± 1.4
1E0920.6+7838	...	G6 V	6.57	1.54 ± 0.62	< 10
1E0307.5+1424	...	G6 V	5.72	1.66 ± 0.71	< 10
1E0257.4+0733	18632	G6 III	93.24	45.77 ± 42.76	< 10
1E0810.2+6305	SAO14468	G7 V-IV	7.65	1.14 ± 0.49	< 10
1E1350.8+1810	121107	G8 III	101.30	10.56 ± 9.91	...
1E0300.2−1528	18955	G8 V	5.67	0.40 ± 0.18	13 ± 0.5
1E0234.8−0210	...	G9 V	5.17	3.93 ± 1.52	< 10
1E1559.9+4202	...	G9 III	124.05	232.31 ± 220.57	< 10
1E0337.6−0202	22853	G9 V	5.17	0.32 ± 0.30	< 10
1E2349.8−0112	...	K0 III	121.79	1084.55 ± 1023.69	50 ± 5.0
1E0657.6+7529	51066	K1 V	5.15	0.55 ± 0.51	43 ± 1.4
1E1810.4+6940	167605	K2 V	4.96	0.67 ± 0.25	< 10
1E0255.3+2018	...	K3 PMS	203.05	4224.45 ± 3951.73	30 ± 3.5
1E1601.1+4119	...	K3 V	5.05	13.39 ± 5.72	< 10
1E0039.2−0206	...	K4 VI	2.98	0.76 ± 0.33	< 10
1E1019.8−1016	...	K5 V	4.57	0.75 ± 0.32	< 10
1E1709.2+5432	155674	K6 V	5.62	0.28 ± 0.10	< 10
1E1215.1+6932	VV Dra	K7 V	7.61	0.42 ± 0.16	< 10
1E0509.5−1607	...	K7 V	7.11	14.05 ± 13.55	11 ± 1.0
1E2253.8+2036	...	K7 V	4.48	10.01 ± 9.29	37 ± 4.5
1E0443.8−1006	...	K7 V	6.48	1.22 ± 0.49	< 10
1E0318.6−1926	...	K7 V	6.79	1.84 ± 0.70	11 ± 1.0
1E0233.8+0649	...	K7e V	4.48	2.23 ± 1.29	12 ± 1.5
1E0444.9−1000	...	M0 V	2.75	5.87 ± 3.42	...
1E1640.1+5349	...	M0e V	3.82	0.87 ± 0.49	< 10
1E1255.3+3529a	GL 490A	M0e V	8.16	1.11 ± 0.30	< 10
1E1404.5+5502	...	M0e V	4.11	6.05 ± 3.51	22 ± 4.3
1E2346.9+1842a	...	M0e V	4.20	2.20 ± 1.27	< 10
1E1224.7+7531	...	M0e V	5.20	0.77 ± 0.45	< 10
1E2332.5+0119	GL 900	M1 V	5.94	0.38 ± 0.15	< 10
1E1441.4+5222	...	M1.5e V	3.89	1.32 ± 0.79	11 ± 1.0
1E1216.1+2818	...	M2e V	2.31	0.94 ± 0.56	21 ± 3.0
1E0816.2+7449	...	M2e V	2.65	0.44 ± 0.25	< 10
1E1112.6+1311	...	M3e V	2.76	1.24 ± 0.74	< 10
1E0401.7+2150a	...	M3e PMS	5.72	11.70 ± 10.82	12 ± 2.0
1E0232.5+2321	...	M3e V	1.28	0.27 ± 0.16	14 ± 4.4
1E2255.7+2039	...	M3e V	3.89	5.02 ± 3.05	18 ± 6.5
1E0401.7+2150b	...	M3e PMS	5.37	11.70 ± 10.82	...
1E0815.3+7433	...	M3e V	2.76	3.66 ± 3.48	...
1E0907.0+0654	...	M4e V	2.20	0.29 ± 0.27	< 10
1E1654.4−0415	LHS 3255	M4e V	1.64	0.30 ± 0.05	< 10
1E1255.3+3529b	GL 490B	M4e V	2.42	1.11 ± 0.30	34 ± 8.5
1E0502.9−1204	LP 716-35	M4e V	2.12	0.09 ± 0.05	< 10
1E0205.5+1454a	...	M4e V	1.64	0.51 ± 0.48	< 10
1E1839.6+8002	LP 25-2	M4e V	1.70	0.22 ± 0.12	< 10
1E1058.2+1220	...	M5e V	0.67	0.09 ± 0.09	...
1E0241.7+1045b	...	M5e V	0.64	0.42 ± 0.39	17 ± 4.1
1E0234.4+0641	...	M5e V	0.68	0.07 ± 0.04	...
1E0205.5+1454b	...	M5e V	0.63	0.13 ± 0.12	< 10
1E0443.9−0952	...	M5e V	0.80	0.10 ± 0.09	...

TABLE 2

BINARY STARS

EMSS	Other (HD)	Sp. Type	R (10^5 km)	L_x (10^{29} ergs s^{-1})	v sin i (km s^{-1})
1E0842.7+1900	74607	F2 V	12.75	1.13 ± 1.07	< 10
1E1440.4+5213	129674	F3 V	12.18	1.73 ± 1.63	70 ± 11.7
1E1208.6+3924	105881	F5 V	9.11	0.94 ± 0.37	...
1E0105.3+3144	6680	F5 IV	13.17	0.92 ± 0.37	68 ± 20.5
1E0002.9+1602	42	F5 V	11.26	5.85 ± 2.34	12 ± 2.0
1E1737.3+6847	160922	F5 V	11.63	1.10 ± 0.26	< 10
1E2119.7+1655	...	F6 V	10.46	35.05 ± 33.27	100 ± 10
1E0730.3+6546	59581	F6 V-IV	10.46	6.45 ± 5.97	17 ± 1.1
1E1222.5+2549	108102	F7 V	8.31	6.43 ± 2.54	...
1E0451.7−0305	...	F8 V	9.54	3032.96 ± 2849.09	...
1E0824.0+2944	71208	F8 V	9.54	2.66 ± 2.49	< 10
1E2038.3−0046	197010	F8 V	9.54	18.57 ± 17.12	100 ± 10
1E0134.4+2027	9902	F9 V	5.62	3.16 ± 1.18	11 ± 0.4
1E1806.1+6944	...	F9 V	7.24	3.89 ± 1.53	100 ± 10
1E0438.6+0213	...	F9 V	9.76	17.86 ± 16.69	...
1E1615.0+3114	...	G0 V	7.41	24.43 ± 9.96	95 ± 10
1E1127.9−1502	100022	G0 V	7.41	9.44 ± 8.90	21 ± 3.0
1E1213.9+3809	...	G2 IV	15.98	968.23 ± 918.32	11 ± 1.8
1E1654.0+3515	...	G2 V	7.30	3.36 ± 1.39	95 ± 10
1E1441.7+5208	129920	G2 V	6.66	1.14 ± 0.44	< 10
1E2116.7−1042	...	G2 V	5.29	7.23 ± 3.18	60 ± 7.6
1E0009.9+1417	SAO91772	G5 V	4.05	3.46 ± 1.36	22 ± 3.0
1E1022.6+1121	...	G6 V	5.47	10.29 ± 4.28	58 ± 9.7
1E1049.5−0849	...	G7 V	6.22	11.63 ± 11.02	...
1E1211.8+1206	106400	G8 V	5.42	2.53 ± 0.98	110 ± 10
1E0244.9−0024	SAO130113	G9 V	4.72	4.27 ± 1.69	17 ± 1.0
1E0505.0−0527	...	G9 IV	3.58	23.85 ± 8.83	14 ± 0.7
1E0348.2−1404	...	K0 IV	4.92	4.68 ± 1.99	< 10
1E0011.6+0840	...	K0 V	3.25	3.99 ± 1.65	22 ± 4.4
1E1520.8−0625	136905	K0 III	121.79	62.39 ± 58.59	35 ± 2.5
1E0657.5+7518	SAO6052	K1 IV	20.49	5.77 ± 5.42	< 10
1E0801.7+2425	...	K1 V-IV	4.69	8.50 ± 3.48	< 10
1E0234.2−0321	16287	K2 V	4.83	0.20 ± 0.09	< 10
1E1559.8+1753	...	K3 V	4.20	1.03 ± 0.43	< 10
1E2148.3+1420	...	K3 V-IV	4.94	56.91 ± 54.23	< 10
1E2113.4+0517	...	K4 V-IV	8.50	12.60 ± 5.22	< 10
1E1533.0+0919	...	K4e V	5.01	3.73 ± 1.57	30 ± 3.0
1E1548.8+1125	...	K5 V-IV	5.01	10.74 ± 4.23	30 ± 3.0
1E0315.8−1955	...	K5 V	7.24	4.67 ± 1.81	23 ± 1.5
1E0924.3+3942	GL 343.1	K8 V	4.57	0.27 ± 0.08	< 10
1E1530.6+1342	...	K8 V	5.64	13.88 ± 7.95	21 ± 2.6
1E0429.4+1755	...	K8e PMS	13.60	23.44 ± 21.88	< 10
1E1050.2−0925	...	M0e V	4.15	2.57 ± 2.44	11 ± 1.2
1E0241.7+1045a	...	M0e V	3.78	1.55 ± 0.88	28 ± 2.6
1E1457.0+2226	...	M2e V	3.13	3.29 ± 1.85	20 ± 3.2
1E2346.9+1842b	...	M3e V	2.24	1.29 ± 0.74	21 ± 4.8

behave like those from Pallavicini *et al.*, i.e., they also fall below the $(v \sin i)^2$ relation.

Taking the EMSS data points in Figure 1*b* which lie above $v \sin i = 10$ km s^{-1}, we calculated two statistical parameters to test the significance of correlation: the linear correlation coefficient (Pearson's r) and the Spearman rank-order coefficient (r_s), as described by Downie and Heath (1965). The results ($r = 0.497$; $r_s = 0.349$) indicate that the null hypothesis which states that L_x and $v \sin i$ are uncorrelated [$h_0(L_x, v \sin i)$] can be rejected at the 99% and 94% confidence levels, respectively.

Assuming that L_x and $v \sin i$ are correlated, we fitted a power-law relation to the EMSS data using the method of least-squares and taking into account the observational errors in both quantities. The result was

$$L_x \propto (v \sin i)^{1.03 \pm 0.24},$$

where $\chi_\nu^2 = 2.56$. When one includes the stars which have upper limits on $v \sin i$ by assigning values of $v \sin i = 5 \pm 5$ km s^{-1} to them, the best fit is

$$L_x \propto (v \sin i)^{1.05 \pm 0.08},$$

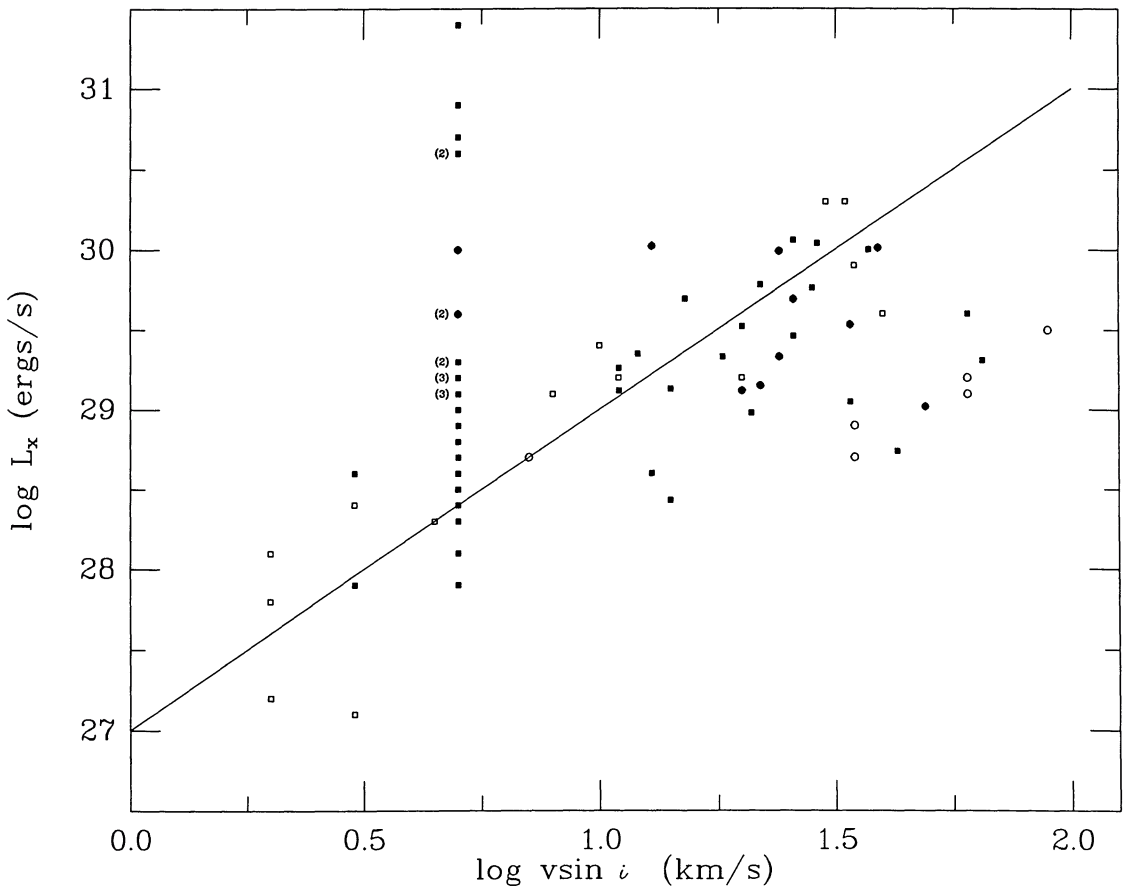

FIG. 1a

FIG. 1.—(*a*) Soft X-ray luminosity vs. projected rotational velocity for all single stars from the EMSS subsample. All stars which have $v \sin i < 10$ km s^{-1} are plotted in one bin at $v \sin i = 5$ km s^{-1}. Stars of spectral type F0–F6 are represented as solid dots, while those of spectral type F7–M5 are represented as solid squares. Also plotted are the late-type stars from Pallavicini *et al.* (1981; F0–F6 are open dots and F7–M5 are open squares). The solid line represents the $L_x \propto (v \sin i)^2$ relation of Pallavicini *et al.* Small numbers in parentheses indicate overprinted points. (*b*) Soft X-ray luminosity vs. projected rotational velocity for all single stars from the EMSS subsample. All stars which have $v \sin i < 10$ km s^{-1} are plotted in one bin at $v \sin i = 5$ km s^{-1}. Only spectral types F7–M5 are plotted (*solid squares*). Also plotted are the late-type stars from Pallavicini *et al.* (1981; *open squares*). The solid line represents the $L_x \propto (v \sin i)^2$ relation of Pallavicini *et al.* The dashed line represents the $L_x \propto v \sin i$ relation which was fitted to the EMSS data.

where $\chi_\nu^2 = 4.09$. This fit is shown in Figure 1*b*. The low-velocity points do not alter the slope for the EMSS sample.

In an attempt to look for correlations with rotational period, however, we found a quite different result. Using the information in Popper (1980), along with color and absolute magnitude, we estimate the radius of each star. Then, the projected angular rotational velocity, $\Omega \sin i$, was calculated for each star by dividing $v \sin i$ by the radius. A plot of L_x versus $\Omega \sin i$ is shown in Figure 2. The statistical correlation parameters ($r = 0.109$; $r_s = 0.077$) indicate that $h_0(L_x, \Omega \sin i)$ can only be rejected at the 43% and 31% confidence levels, respectively. In essence, L_x does not correlate with $\Omega \sin i$.

As a check, we also estimated the radius of and calculated $\Omega \sin i$ for each late-type star in the Pallavicini *et al.* sample in the same manner. The statistical correlation parameters of L_x versus $\Omega \sin i$ for the Pallavicini *et al.* sample ($r = 0.465$; $r_s = 0.363$) indicate that $h_0(L_x, \Omega \sin i)$ can be rejected at the 94% and 85% confidence levels, respectively. This confirms that L_x probably does correlate with rotation for the stars in the Pallavicini *et al.* sample.

Therefore, the correlation seen between L_x and $v \sin i$ for the stars in our EMSS subsample must, in reality, be a correlation of L_x with radius and not rotation. In order to investigate the physical significance of this correlation, we plot L_x versus radius for all single stars in our EMSS subsample in Figure 3. The statistical correlation parameters ($r = 0.794$; $r_s = 0.672$) indicate that $h_0(L_x, R)$ can be rejected at the 99.9% confidence level in both cases.

Before deciding whether the observed correlation between L_x and radius in the EMSS late-type stars is real or artificially induced, one must consider the empty regions of Figure 3. First, there is the lower, right-hand corner which represents stars of large radius (e.g., massive dwarfs and giants) and low X-ray luminosities. In order to be detected by the EMSS, stars with low L_x must be in the solar neighborhood. However, F and G dwarfs and giants are rare within 25 pc of the Sun. Therefore, the sensitivity limit of the EMSS would prevent the detection of such stars. Second, the upper, left-hand region of Figure 3 represents stars of small radius (e.g., low-mass dwarfs) and high X-ray luminosities. At such high values of L_x, a star could be detected in the EMSS for hundreds of parsecs from the Sun, a volume of space which contains plenty of low-mass dwarfs (i.e., the low-mass dwarfs are much more numerous per unit volume than the higher mass stars which were detected.) Therefore, it is clear that the upper, left-hand region of Figure 3 is truly empty, whereas the lower, right-hand region may

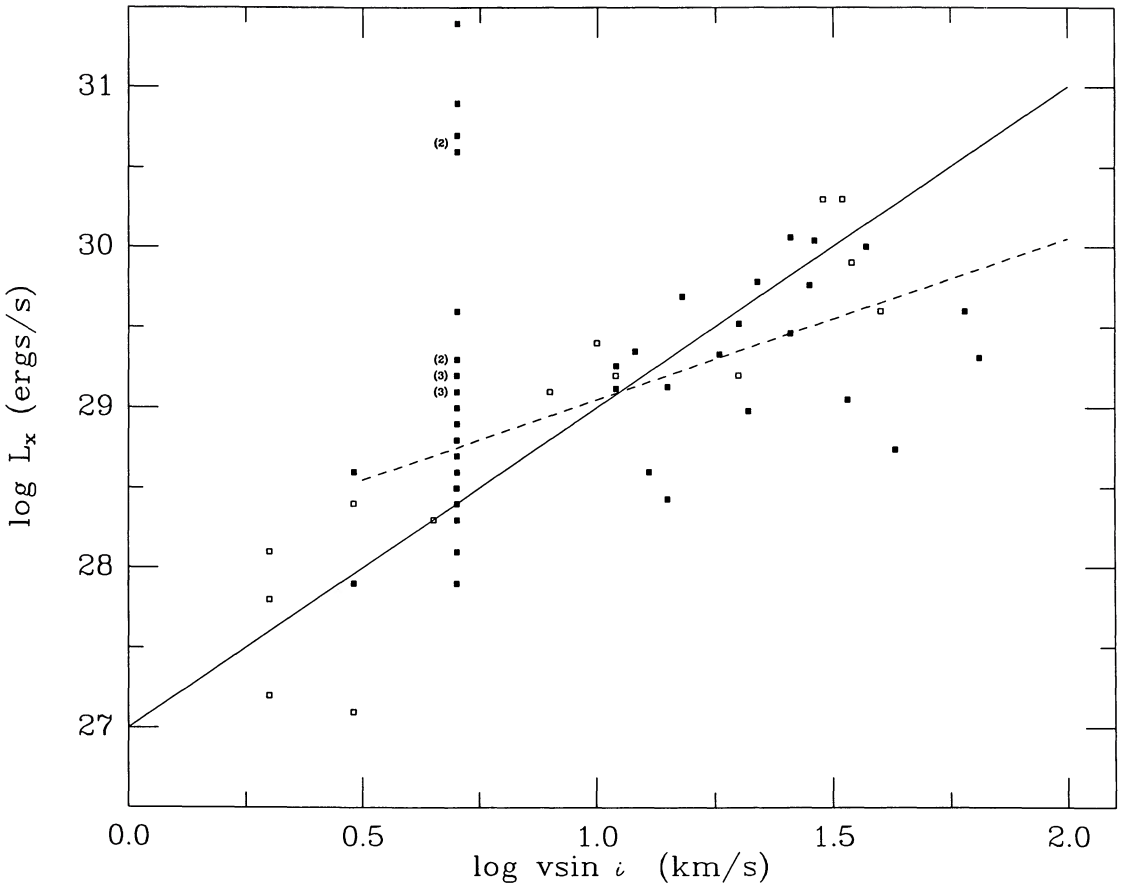

FIG. 1*b*

contain points which represent stars beyond the EMSS detection limit.

The points in Figure 3 have also been coded by rotation. One can see that the slow rotators generally have lower values of L_x than the rapid rotators except for the F stars ($R \sim 10^6$ km), where all rotation rates are mixed vertically in the diagram. This implies that L_x is a function of two parameters: rotation and radius (or mass, color, convection zone depth, etc.). L_x increases with rotation until it reaches a limiting value. The upper limit on L_x is a function of radius, increasing with increasing radius. An X-ray–selected sample is better suited than all other types of samples for defining this upper limit. One cannot formally fit a boundary to a set of data, but we have drawn a line on Figure 3 (with a slope of 2) which nicely follows the trend in the data. It is highly suggestive that the upper boundary to the data in Figure 3 (the saturation luminosity, $L_x^{(\mathrm{sat})}$, which is described later in this paper) may have the following functional form:

$$L_x^{(\mathrm{sat})} \propto R^2 \propto M^2 ,$$

since R is nearly proportional to M along the main sequence.

If all late-type stars could be represented in Figure 3, the collection of all points would not strongly correlate with radius, unlike the upper limit on L_x. But since the EMSS subsample is X-ray–selected, it preferentially detects stars which lie along the upper boundary. Therefore, the correlation seen in Figure 3 is artificially induced by an observational selection effect. This permits us to understand better how the physics of saturation depends on various stellar parameters.

b) Binary Stars

The L_x versus $v \sin i$ diagram for those EMSS stars in astrophysical binary systems is shown in Figure 4*a*. An examination of this figure reveals the fact that narrow-lined, as well as rotationally broadened, spectra are seen among the binaries. Is this what one would expect from a synchronously rotating system? The primary should rotate with a period equal to the orbital period which, in the case of these binaries, is typically less than 10 days. An angle of inclination effect cannot be used to explain the presence of narrow-lined spectra among these binaries since the very radial velocity variations which identify them as binaries were observed.

The detection of these narrow-lined binaries, which account for 30% (14 out of 47) of the binaries in our EMSS subsample, can be explained if the secondary is a faint Me or Ke dwarf. With a large mass ratio, a synchronous binary system could have a primary with a $v \sin i < 10$ km s^{-1} and still have detectable radial velocity variations. Such a system would be noninteracting and, in all probability, the true source of the X-rays would be the Me or Ke dwarf companion. Support for this hypothesis comes from one example among these binaries which, due to its apparent brightness, is already well-observed. The F5 dwarf ω Draconis (1E 1737.3+6847) is an SB1 whose radial velocity curve is known ($P = 5.28$ days, $k = 35.4$ km

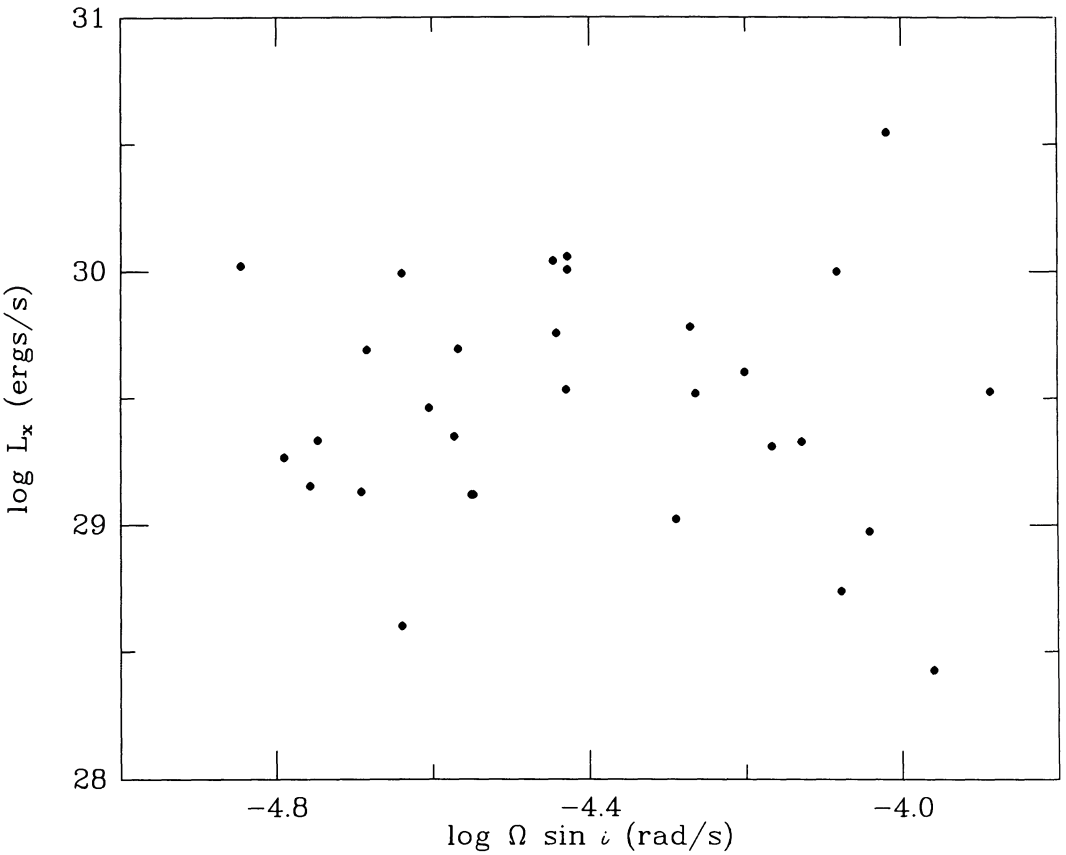

FIG. 2.—Soft X-ray luminosity vs. projected angular rotational velocity for those single stars from the EMSS subsample which have $v \sin i > 10$ km s^{-1}. Only spectral types F7–M5 are plotted. These data are statistically uncorrelated.

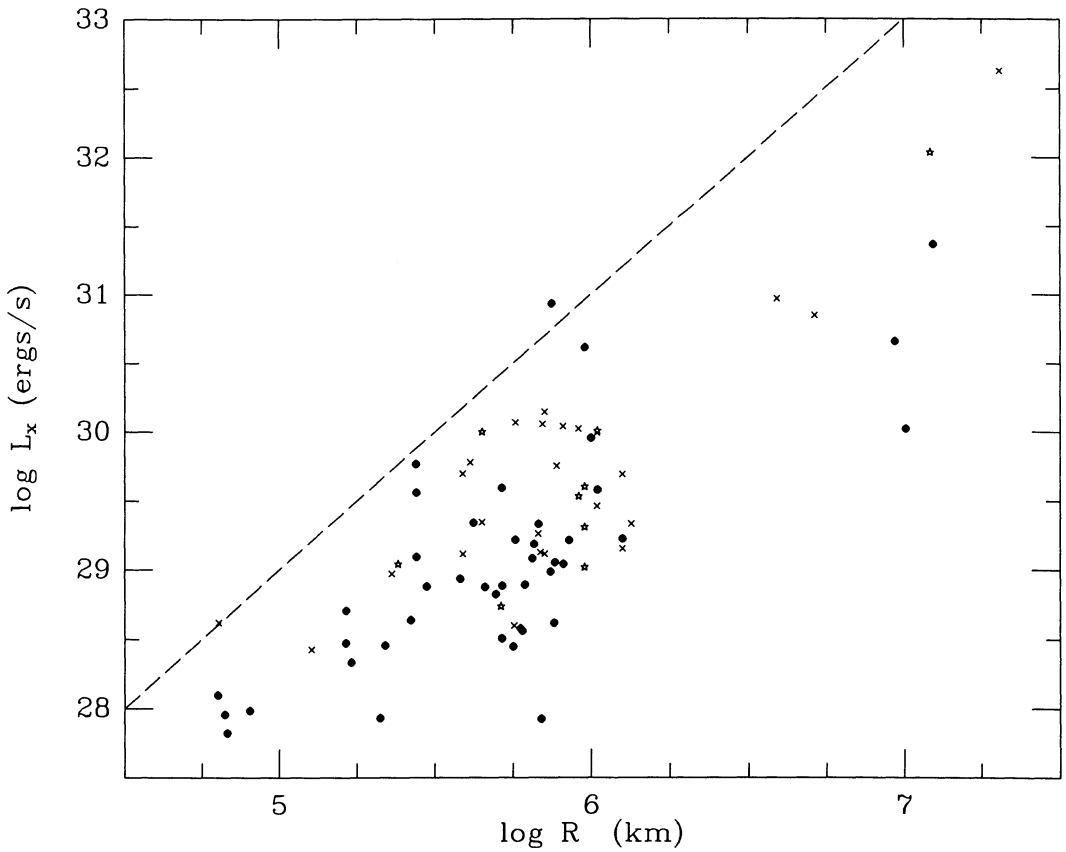

FIG. 3.—Soft X-ray luminosity vs. stellar radius for all single stars in the EMSS subsample. The symbols are coded by rotation as follows: stars—$v \sin i > 40$ km s^{-1}; crosses—$40 > v \sin i > 10$ km s^{-1}; solid dots—$v \sin i < 10$ km s^{-1}; open dots—no rotation measurement. The dashed line represents the plausible saturation boundary of $L_x^{(\mathrm{sat})} \propto R^2$.

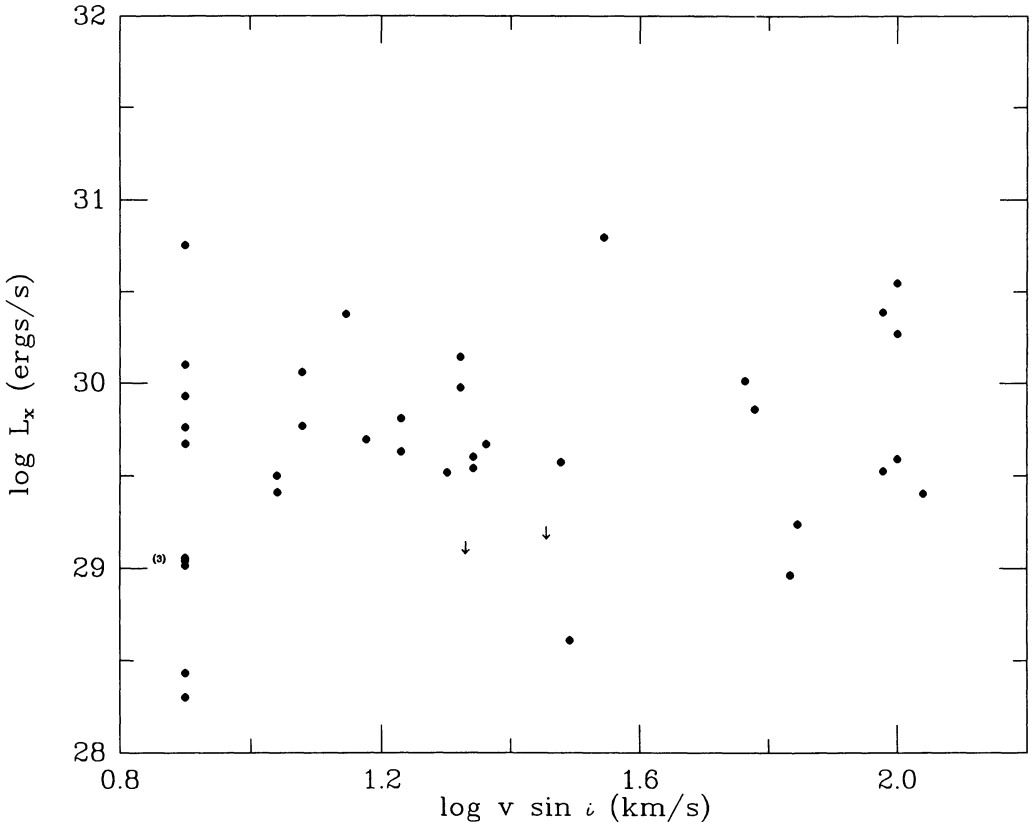

FIG. 4*a*

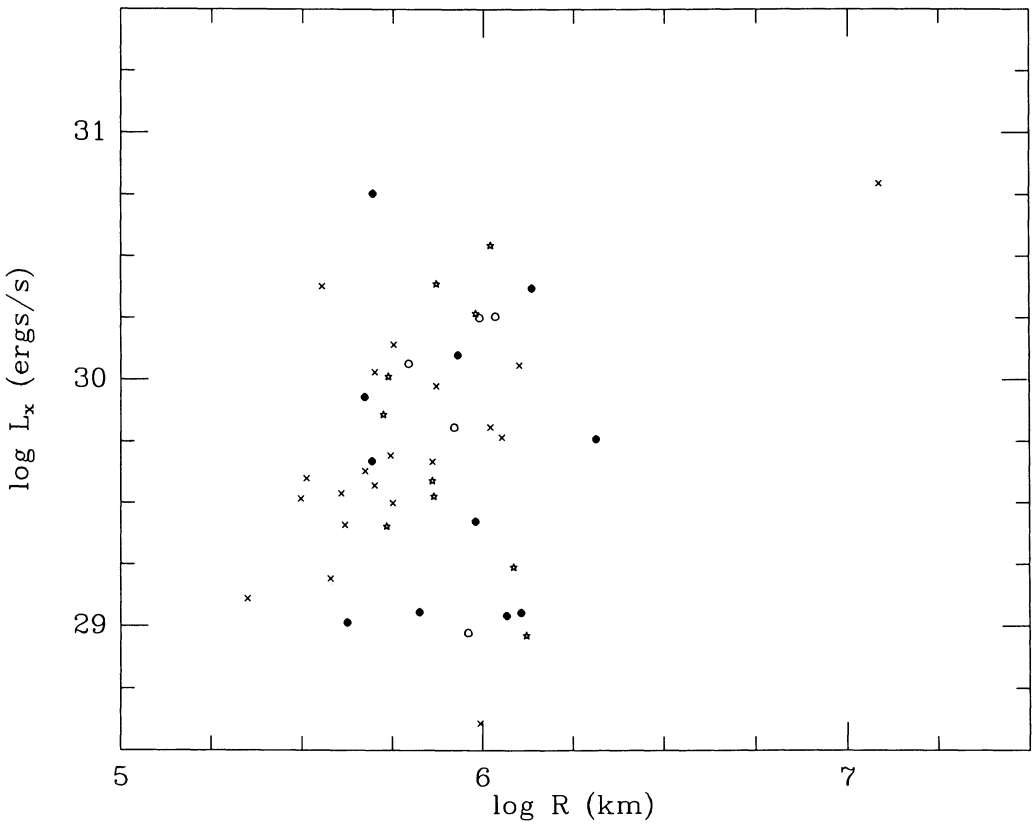

FIG. 4*b*

FIG. 4.—Soft X-ray (0.3–3.5 keV) luminosity vs. projected rotational velocity for the binaries from the EMSS subsample. This plot includes only stars of spectral type F0–M5 and excludes pre–main-sequence stars. All stars which have $v \sin i < 10$ km s^{-1} are plotted in one bin at log $v \sin i = 0.9$. Upper limits on L_x due to ambiguous detections are indicated by arrows. (*b*) Soft X-ray luminosity vs. stellar radius of the primary for all binaries in the EMSS subsample. The symbols are coded by rotation as follows: stars—$v \sin i > 40$ km s^{-1}; crosses—$40 > v \sin i > 10$ km s^{-1}; solid dots—$v \sin i < 10$ km s^{-1}; open dots—no rotation measurement.

s^{-1}; Abt and Levy 1976). A typical mass and radius for an F5 dwarf are 1.3 $M_\odot$ and 1.2 $R_\odot$, respectively. Suppose that this F5 dwarf is synchronously orbiting with an M2 dwarf (0.42 $M_\odot$). Then, the rotational velocity of the F5 dwarf, derived from the equation: $v_{rot} = 2\pi R/P$, should be 11.5 km s^{-1}. This result is entirely consistent with the observed $v \sin i < 10$ km s^{-1}. The amplitude of the radial velocity variation can be estimated by rewriting Kepler's Third Law in the form $v_{rel} = (M/P)^{1/3}$, where M is the total mass of the system in units of $M_\odot$, P is the period in units of days, and $v_{rel} = v_{primary}/\mu$ is in units of 213 km s^{-1}. The reduced mass, μ, of this system is 0.24. Substituting the values given above into this relation, we calculate $v_{primary}$ (the amplitude of radial velocity variation of the primary) to be 35.2 km s^{-1}, which is in excellent agreement with the observations. Therefore, it is reasonable to assume that ω Draconis has an M dwarf companion. We further suggest that this is probably also true for the other narrow-lined binaries in our EMSS subsample.

Among the binaries in the subsample which exhibit rotationally broadened line profiles, 34% appear to be of the RS CVn type. W UMa type binaries account for 13%, Me dwarfs for 9%, and Ke dwarfs for another 9%. There are also two cataclysmic variables and one pre-main sequence star among the binary sample (not shown in Fig. 4*a*).

For those binaries with measurable rotational velocities, the statistical correlation parameters ($r = -0.023$; $r_s = 0.050$) indicate that $h_0(L_x, v \sin i)$ can only be rejected at the 9% and 19% confidence levels, respectively. X-ray luminosity does not correlate with $v \sin i$. Not even the induced correlation with radius is seen, as it is in the case of the single stars (Fig. 1).

However, L_x may correlate with radius. This is not immediately evident from a visual inspection of Figure 4*b*, where L_x is plotted against the radius derived from the primary component. But the statistical parameters ($r = 0.317$; $r_s = 0.260$) indicate that $h_0(L_x, R)$ can be rejected at the 98% and 93% confidence levels, respectively. It appears that the upper boundary on L_x for the binaries may also be a function of radius (or mass, color, etc.). Unfortunately, the binary star data which is displayed in Figure 4*b* spans a smaller range in radius than the single star data in Figure 3.

Furthermore, no great separation is seen in Figure 4*b* between stars of different rotation rates. However, we emphasize an important caveat regarding the measurement of $v \sin i$ for the binary stars. If the system is a single-line spectroscopic binary, then the observed line broadening will be caused by the rotation of the primary. But if the system is a double-line spectroscopic binary which is spectroscopically blended (i.e., a wide pair having small velocity separation), then the line widths will vary from epoch to epoch as the radial velocity of each component changes. Consequently, $v \sin i$ values measured from line widths could overestimate rotation. We fail to note $v \sin i$ for those binaries whose cross-correlation peak width (i.e., echelle spectral line broadening) varied from epoch to epoch.

IV. ROTATIONAL SATURATION

The results presented above for the single stars constitute the best observational evidence yet for rotational saturation in the coronae of late-type stars. Unlike previous samples of stars which have been used to support this idea (e.g., Vilhu and Walter 1987), the EMSS subsample was selected to contain the brightest X-ray sources among all types of stars in a completely unbiased (except, of course, for X-rays) manner.

The concept of rotational saturation in coronal, as well as chromospheric, heating has been suggested by several authors to explain the breakdown of the functional dependence between coronal and chromospheric flux and rotation (or Rossby number) at high rotation rates (Vilhu and Walter 1987; Skumanich 1986; Skumanich and MacGregor 1986; Vilhu 1984). The basic argument involves the limited area of the stellar surface. As more surface field is generated with increasing rotation, a point is eventually reached where the stellar surface is totally covered with active regions. The footpoints of magnetic loops crowd each other out, and no new loops can be created. Consequently, nonradiative coronal heating reaches a maximum value, and so does X-ray emission. This would explain the dependence of the upper limit to L_x on radius in Figure 3. This boundary is scaling with surface area.

Another idea involves magnetic feedbacks in the convection zone (cf. Gilman 1983). As increased angular velocity causes the generation of stronger magnetic fields, the Lorentz forces which result act to decrease differential rotation and inhibit convection in the zone. This, in turn, will decrease magnetic field strength until the differential rotation increases again. This cyclical process would effectively limit the extent to which a corona could be heated. Such an upper boundary would be a function of convection zone parameters and, hence, mass, color, radius, etc.

The observational results presented above are, by themselves, insufficient to prove conclusively that stellar coronae saturate at high rotational velocities. Ideally, one would wish to plot L_x versus v_{rot} for each star and to normalize both parameters by the saturation value of that parameter which one would expect given each star's radius (mass). Then, all stars would fall on the same locus of positive slope, increasing to unity and then flattening out to a slope of zero. Unfortunately, the saturation values of L_x and v_{rot} as a function of stellar radius (mass) are not determined. In Figure 5, we attempt to approximate the plot described above by using both L_x/L_{bol} (Fig. 5*a*) and X-ray surface flux, F_x (Fig. 5*b*) as surrogates for $L_x/L_x^{(sat)}$. Both quantities are plotted against an unnormalized $v \sin i$, so we have coded each point by spectral type since one would expect the points which represent stars of different masses to fall along separate loci.

In both figures, the distribution of points for all spectral types (except perhaps type M) is quite flat. If rotational saturation of stellar coronae is indeed a real effect, then it appears that X-ray selection has given us a sample which only falls along the flat part of the curve which was described in the last paragraph. However, it is interesting to compare the dispersion of the data points in Figures 5*a* and 5*b*. The values of L_x/L_{bol} spread slightly over three orders of magnitude, while the spread in F_x is only one and one-half orders of magnitude. Furthermore, the mean values of L_x/L_{bol} and F_x for each spectral type are given in Table 3. The values in Table 3 range over almost two orders of magnitude for L_x/L_{bol}, while the values for F_x are within a factor of 2. This suggests that surface area ($4\pi R^2$) is a better surrogate than L_{bol} for $L_x^{(sat)}$ (if it exists).

We have already characterized the saturation boundary in terms of L_x ($L_x^{(sat)} \propto R^2$). Given this and the preceding discussion, one would expect $F_x^{(sat)}$ to be constant as a function of stellar radius (mass). In Figure 6, we plot F_x versus $B-V$ color for both single stars and binaries following Figure 6 of Vilhu and Walter (1987). We use $B-V$ color as the abscissa of Figure 6 for ease of comparison to the results of Vilhu and Walter. The dashed lines represent their X-ray upper bound for $0.1 < B-V < 0.6$ and the locus of $F_x/F_{bol} = 10^{-3}$, about

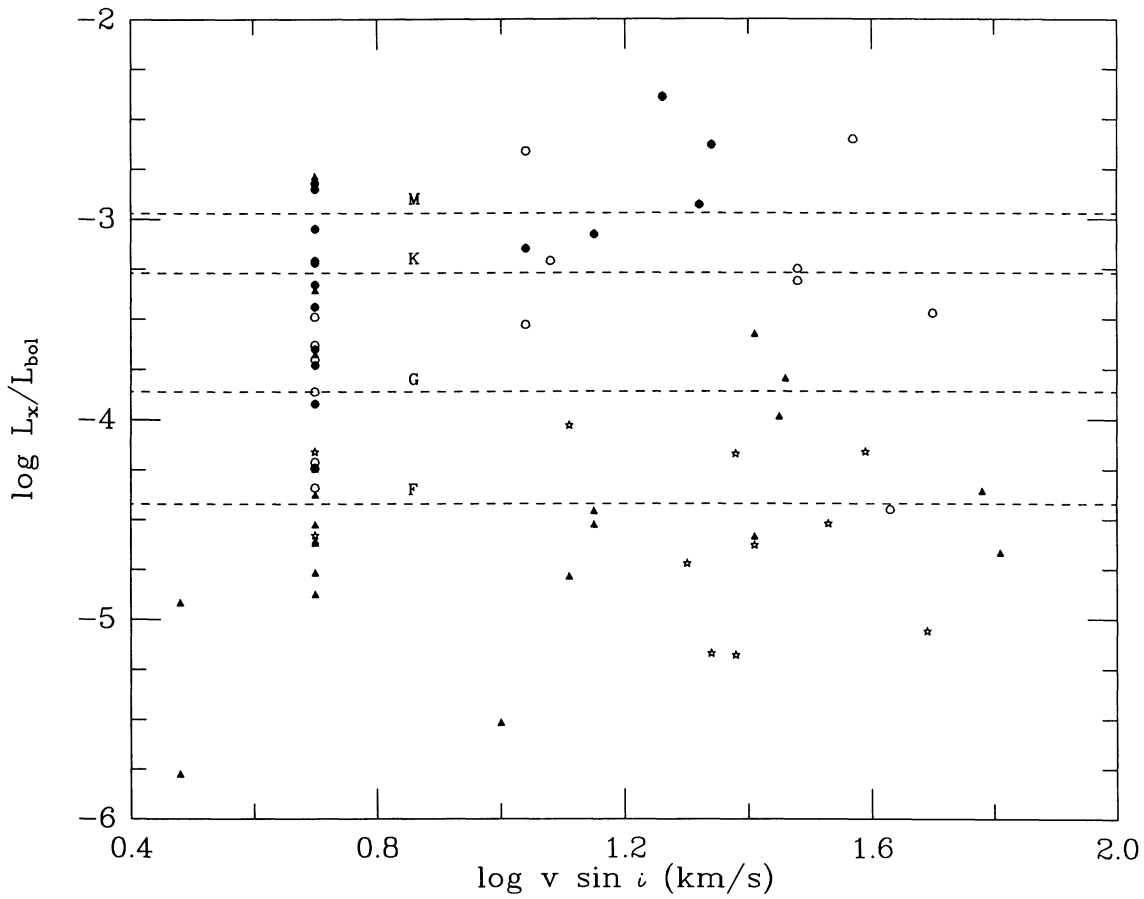

FIG. 5*a*

FIG. 5.—(*a*) Fractional X-ray luminosity vs. projected rotational velocity for all single stars from the EMSS subsample (excluding ambiguous detections and PMS). Solid dots represent type M, open dots represent type K, triangles represent type G, and stars represent type F. The dashed lines indicate $\langle L_x/L_{bol}\rangle$ for each spectral type (from Table 3). Note the wider spread in the ordinate compared to Fig. 5*b*. (*b*) Soft X-ray surface flux vs. projected rotational velocity for all single stars from the EMSS subsample (excluding ambiguous detections and PMS). Solid dots represent type M, open dots represent type K, triangles represent type G, and stars represent type F. The dashed lines indicate $\langle F_x\rangle$ for each spectral type (from Table 3). Note the narrower spread in the ordinate compared to Fig. 5*a*.

which most of their M dwarfs fell. The dotted lines represent the loci of $F_x/F_{bol} = 10^{-2.5}$ and 10^{-2}. The EMSS stars lie below their upper bound for the bluer stars, but our sample contains many more K and M stars which reach fractional X-ray luminosities as high as $10^{-2.5}$.

The upper bound on F_x ($F_x^{(sat)}$) appears to increase steadily with color until one reaches $B-V = 0.6$; then it appears that F_x levels off to a constant value ($\sim 7 \times 10^7$ ergs s^{-1} cm^{-2}) at $B-V > 0.6$. This constant value represents the point at which the coronal heating mechanism operates at its greatest efficiency. Since F_x is normalized by surface area, $F_x^{(sat)}$ is not directly determined by the radius (such as $L_x^{(sat)} \propto R^2$). The fundamental question which is answered by deciding whether $F_x^{(sat)}$ is constant or $(F_x/F_{bol})^{(sat)}$ is constant (i.e., $F_x^{(sat)} \propto \sigma T_{eff}^4$) is this. Does stellar X-ray emission at saturated levels depend upon the internal energy source, or is it determined purely by surface area?

The steady decrease in $F_x^{(sat)}$ as a function of increasing stellar mass for $B-V < 0.6$ results from the decrease in convection zone depth. According to the magnetic dynamo scenario, poloidal magnetic field is created from the turbulent twisting of the toroidal field which is buoyantly rising through the convection zone (the α-effect). This poloidal magnetic field reinforces the original fields from which the toroidal magnetic field was first created (the Ω-effect) and feeds the dynamo. If the convection zone depth is too shallow (i.e., convective turnover time is too short), then the toroidal magnetic field will float to the stellar surface before the α-effect has had time to operate. Thus, the dynamo mechanism and the associated nonradiative coronal heating process are apparently less efficient.

TABLE 3

MEAN CORONAL EMISSION PARAMETERS OF SINGLE STARS BY SPECTRAL TYPE

Parameter	M	K	G	F
$\langle L_x/L_{bol}\rangle$	1.06×10^{-3}	5.40×10^{-4}	1.37×10^{-4}	3.83×10^{-5}
$\langle F_x\rangle$ (ergs cm^{-2} s^{-1})	1.10×10^7	7.31×10^6	9.97×10^6	4.09×10^6

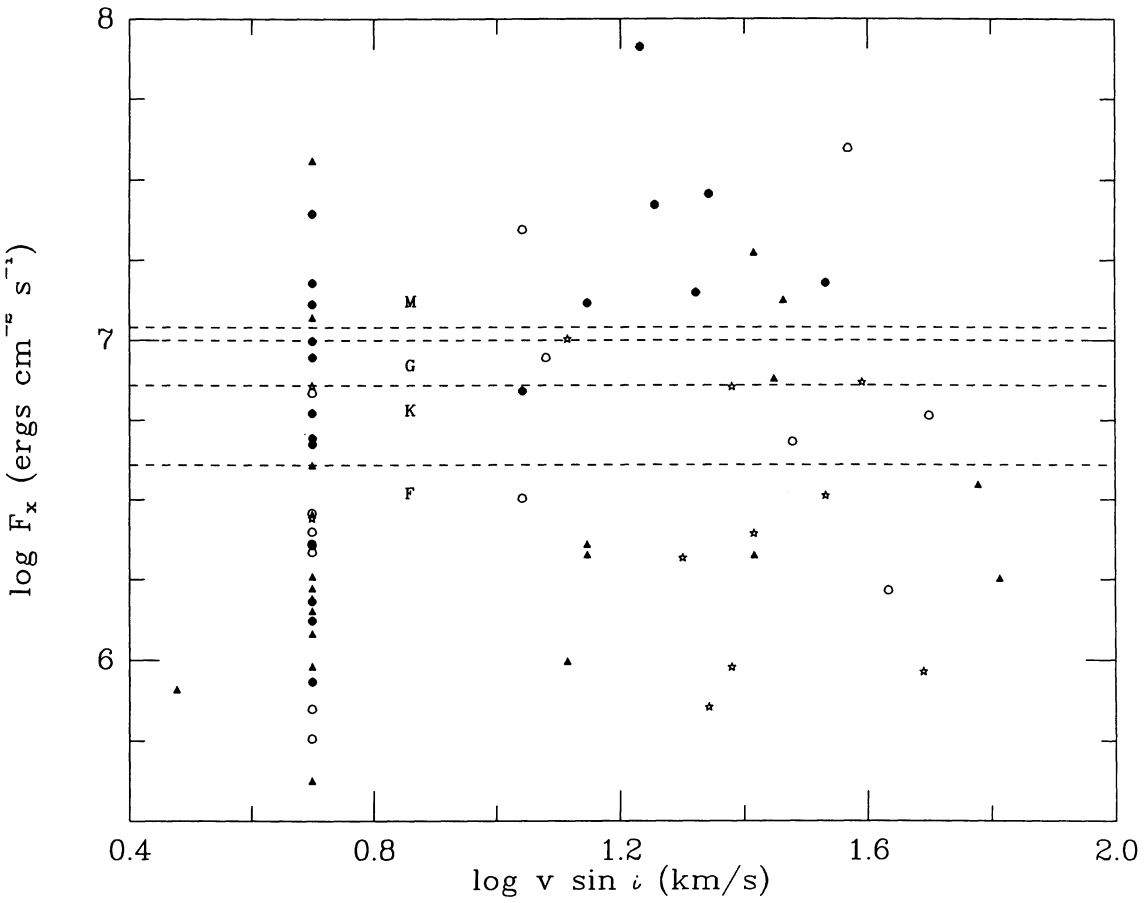

FIG. 5*b*

This could explain why the F stars are underluminous in X-rays at high rotation rates, as illustrated in Figure 1*a*.

As for the binaries, their saturation limit in F_x appears to be similar to that of the single stars. The situation for the binaries is more complicated, however, when one considers that the X-ray–emitting region is not just the surface area of the primary, but also that of the secondary and the intervening area as well. A complete analysis of these X-ray–selected binaries must await the determination of their periods, when one can then draw more significant astrophysical conclusions.

V. SUMMARY

We have presented X-ray and rotational data for an X-ray–selected, flux-limited sample of 128 late-type stars. This is the largest and best optically observed X-ray–selected sample to date. For single stars of spectral types F7–M5, $L_x \propto (v \sin i)^{1.05 \pm 0.08}$ but does not correlate with $\Omega \sin i$. Stars of spectral types F0–F6 are slightly underluminous in X-rays for this relation. However, L_x does correlate with radius for these stars.

These results appear to contradict the earlier work of Pallavicini *et al.* (1981), but in reality they do not. The Pallavicini *et al.* sample was optically selected and, hence, more representative of stars at all levels of activity. It could well be that $L_x \propto (v \sin i)^2$ for stars which are at levels below saturated activity. Our X-ray-selected sample is more representative of the highest levels of X-ray activity, which do appear to saturate. These stars lie along the upper limit on L_x, which is a function of surface area, and thus a strong correlation of L_x with radius is artificially induced. When one normalizes L_x by the surface area (F_x), one finds that $F_x^{(\mathrm{sat})}$ increases with color until $B-V = 0.6$, where it appears to level off at a constant value ($F_x \sim 7 \times 10^7$ ergs cm^{-2} s^{-1}). Although these results do not conclusively prove that rotational saturation in stellar coronae is a real effect, they do indicate that it is plausible. Furthermore, these data (especially as presented in Figs. 3 and 5) suggest that saturation in L_x is a geometric effect caused by limited surface area. The value of $L_x^{(\mathrm{sat})}$ depends most strongly upon radius, rather than T_{eff}.

The L_x for binaries from this sample correlates with neither $v \sin i$ nor $\Omega \sin i$, but it may correlate with radius. This behavior is different from that of the single stars because the situation in binary systems is more complicated. One must consider emission from both components and the area in between.

This work was part of a Ph.D. dissertation at the University of Arizona. T. F. would like to acknowledge members of his committee for many useful comments: J. Liebert, R. F. Green, M. Giampapa, S. White, and R. E. White, Jr. We thank L. Hartmann for advice on the measurement of rotational velocities; D. Latham, R. Peterson, and R. Stefanik for assistance with the reduction and analysis of the echelle data; and J. Stocke, S. Morris, and E. M. Green for collaboration in obtaining the optical data. We also thank F. R. Harnden, Jr. and H. Tananbaum for critical readings of the manuscript. This work was partially supported by NASA grants NAG8-666 and NAS8-30751 and by the Smithsonian Scholarly Studies grant SS88-03-87.

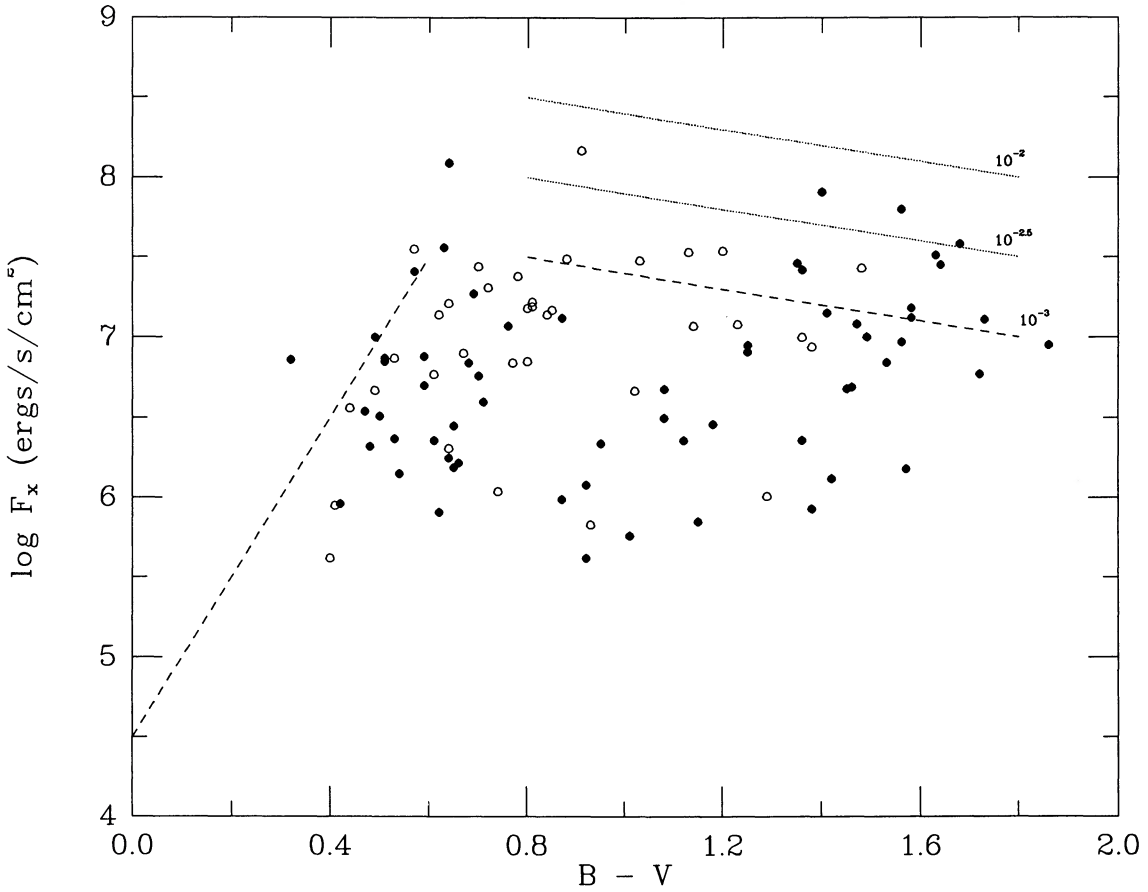

FIG. 6.—Soft X-ray surface flux versus color for all F0–M5 stars from the EMSS subsample. Single stars are plotted as solid dots, while binaries are plotted as open dots. The dashed lines represent the upper bound to F_x for $0.1 < B-V < 0.6$ given by Vilhu and Walter (1987) and the locus of constant $F_x/F_{bol} = 10^{-3}$. The dotted lines represent the loci of constant F_x/F_{bol} values of $10^{-2.5}$ and 10^{-2}.

REFERENCES

Abt, H. A., and Levy, S. G. 1976, *Ap. J. Suppl.*, **30**, 273.
Bessel, M. S. 1976, *Pub. A.S.P.*, **88**, 557.
Boeshaar, P. C. 1976, Ph.D. thesis, Ohio State University.
Bouigue, R. 1973, *Trans. IAU*, **15A**, 409.
Caillault, J.-P., and Helfand, D. J. 1985, *Ap. J.*, **289**, 279.
Caillault, J.-P., Helfand, D. J., Nousek, J. A., and Takalo, L. O. 1986, *Ap. J.*, **304**, 318.
Downie, N. M., and Heath, R. W. 1965, *Basic Statistical Methods* (2d ed.; New York: Harper and Row), p. 206.
Favata, F., Rosner, R., Sciortino, S., and Vaina, G. S. 1988, *Ap. J.*, **324**, 1010.
Fleming, T. A. 1988, Ph.D. thesis, University of Arizona.
Fleming, T. A., Liebert, J., Gioia, I. M., and Maccacaro, T. 1988, *Ap. J.*, **331**, 958.
Gilman, P. 1983, *Ap. J. Suppl.*, **53**, 243.
Gioia, I. M., Maccacaro, T., Schild, R. E., Stocke, J. T., Liebert, J. W., Danziger, I. J., Kunth, D., and Lub, J. 1984, *Ap. J.*, **283**, 495.
Gioia, I. M., Maccacaro, T., and Wolter, A. 1987, in *IAU Symposium 124, Observational Cosmology*, ed. A. Hewitt, G. Burbidge, and Li-Zhi Fang (Dordrecht: Reidel), p. 593.
Gliese, W. 1982, *Astr. Ap. Suppl.*, **47**, 471.
Gorenstein, P., Harnden, F. R., Jr., and Fabricant, D. G. 1981, *IEEE Nucl. Sci.*, **NS-28**, 869.
Hartmann, L., Hewett, R., Stahler, S., and Mathieu, R. 1986, *Ap. J.*, **309**, 275.
Jacoby, G. H., Hunter, D. A., and Christian, C. A. 1984, *Ap. J. Suppl.*, **56**, 257.
Latham, D. W. 1985, in *IAU Colloquium 88, Stellar Radial Velocities*, ed. A. G. D. Philip and D. W. Latham (Schenectady: Davis), p. 21.
Maccacaro, T., Gioia, I. M., Wolter, A., Zamorani, G., and Stocke, J. T. 1988, *Ap. J.*, **326**, 680.
Maccacaro, T., *et al.* 1982, *Ap. J.*, **253**, 504.
Mangenay, A., and Praderie, F. 1984, *Astr. Ap.*, **130**, 143.
Marilli, E., and Catalano, S. 1984, *Astr. Ap.*, **133**, 57.
Micela, G., Sciortino, S., Serio, S., Vaiana, G. S., Bookbinder, J., Golub, L., Harnden, F. R., and Rosner, R. 1985, *Ap. J.*, **292**, 172.
Mikami, T. 1978, *Pub. Astr. Soc. Japan*, **30**, 207.
Pallavicini, R. P., Golub, L., Rosner, R., and Vaiana, G. S. 1982, in *Second Cambridge Workshop on Cool Stars, Stellar Systems, and the Sun* (SAO Special Report 392), ed. M. S. Giampapa and L. Golub, p. 77.
Pallavicini, R. P., Golub, L., Rosner, R., Vaiana, G. S., Ayres, T., and Linsky, J. L. 1981, *Ap. J.*, **248**, 279.
Popper, D. M. 1980, *Ann. Rev. Astr. Ap.*, **118**, 115.
Raymond, J. C., and Smith, B. W. 1977, *Ap. J. Suppl.*, **35**, 419.
Reid, I. N., and Gilmore, G. F. 1982, *M.N.R.A.S.*, **201**, 73.
Rosner, R., Golub, L., and Vaiana, G. S. 1985, *Ann. Rev. Astr. Ap.*, **23**, 415.
Ruciński, S. M. 1984, *Astr. Ap.*, **132**, L9.
Skumanich, A. 1986, *Ap. J.*, **309**, 858.
Skumanich, A., and MacGregor, K. 1986, *Adv. Space Res.*, Vol. **6**, No. 8, p. 151.
Stocke, J. T., Liebert, J. W., Gioia, I. M., Griffiths, R. E., Maccacaro, T., Danzinger, I. J., Kunth, D., and Lub, J. 1983, *Ap. J.*, **273**, 458.
Tonry, J., and Davis, M. 1979, *A.J.*, **84**, 1511.
Turnshek, D. E. 1981, M.S. thesis, University of Arizona.
Turnshek, D. E., Turnshek, D. A., Craine, E. R., and Boeshaar, P. C. 1985, *An Atlas of Digital Spectra of Cool Stars* (Tucson: Western Research Co.).
Vilhu, O. 1984, *Astr. Ap.*, **133**, 117.
Vilhu, O., and Walter, F. M. 1987, *Ap. J.*, **321**, 958.
Walter, F. M. 1982, *Ap. J.*, **253**, 745.
———. 1983, *Ap. J.*, **274**, 794.

THOMAS A. FLEMING: Max-Planck-Institut für Extraterrestrische Physik, 8046 Garching bei München, Federal Republic of Germany

ISABELLA M. GIOIA and TOMMASO MACCACARO: Harvard-Smithsonian Center for Astrophysics, 60 Garden Street, Cambridge, MA 02138